MECHANICS OF CAMBERED WEB BELTS ON ALIGNED ROLLERS

By

J. Shi, J. Smith, R. Markum and J. K. Good
Oklahoma State University
USA

ABSTRACT

The lateral deformations of webs in roll-to-roll (R2R) process machines can affect the quality of the manufacturing process. Webs can enter a cylindrical roller normally if the forces required to sustain normal entry and do not exceed the available friction forces. Webs with simple non-uniform length variation across their width (camber) will steer toward the long side, affecting the steady state lateral deformation and hence registration. Most previous studies have focused on tests and modeling a cambered web span in a free span between two rollers. Often these studies assume some displacement and slope boundary conditions are known and seek the remaining condition(s) that would dictate the steady state lateral deformation of the cambered web in the free span. In many spans in a process machine there may be no known boundary conditions and no steady state deformation of the cambered web. The web may travel toward the long side continually from one web span until the next until a web guide attempts to return the web to an acceptable lateral location in the process machine. The simplest case of multiple span cambered web lateral behavior is that of a cambered web belt transiting two aligned rollers which is the focus of the current work. Dynamic simulation (Abaqus/Standard) has been used to better understand the response of cambered webs under tension that has been witnessed in tests.

INTRODUCTION

All webs have some degree of cross-web length non-uniformity. A web whose length varies linearly across the width in the cross-machine direction (CMD) is said to have constant web camber, the simplest case of web length non-uniformity. Such a web supported on a flat surface and stress-free would have the appearance of a curved beam with constant radius of curvature. The radius of curvature that defines a constant web camber is defined at the elastic axis of the web [1]. If a sector of a cambered web is cut and laid flat on a surface, one edge of the web will be longer than the other edge. Even when the cambered web is in the form of a belt, reference will still be made to the long

and short sides of the web. Some authors also refer to the slack and taut edge of the web. When the cambered web is subject to tension in transit bending stresses result which cause the short side to undergo higher MD stress than that due to web tension. Conversely the long side will have an MD stress lower than that due to web tension. Thus the short or taut edge refers to the same edge and the long or slack edge are also synonymous. When a cambered web is being transported through a web line, a portion of the camber will diminish visibly due to web tension. Camber can result from the process from which the web is made. Most often it is the result of viscoelastic deformation due web thickness non-uniformity in the CMD and residual winding stresses while the web is stored in a wound roll.

The steering behavior cambered webs transiting through roll-to-roll process machines has been explored for over 50 years. Shelton offered cambered web steering as an important problem that should be addressed in 1968 [2]. Tests have consistently shown that camber will result in the web steering beyond the straight path a uniform web would follow toward the long side of the web [1, 3, 4]. To date no closed form expression correctly predicts the lateral steering witnessed in those tests [1, 3-11]. Webs are often treated as beams. In steady state, the lateral deformation of a free span shown in Figure 1 is governed by the differential equation:

$$EI\frac{d^4w}{dx^4} - T\frac{d^2w}{dx^2} = 0 \qquad \{1\}$$

where w is the lateral deformation of web, x is a coordinate on the elastic axis identified in Figure 1, T is the web tension in units of load. EI is the bending stiffness of the web which is the product of Young's modulus E in the x-direction and the area moment of inertia of the web I about the out-of-plane axis.

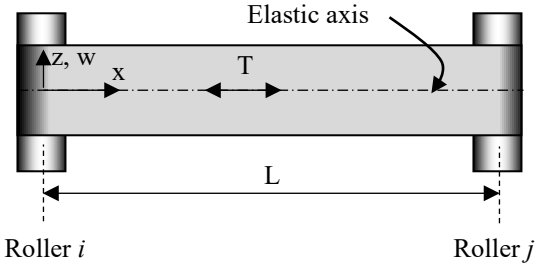

Figure 1 – A web transiting a span length L from roller *i* to *j*

The solution to the differential equation {1} has the form:

$$w = A + B\frac{x}{L} + C*\cosh\left[\frac{\lambda x}{L}\right] + D*\sinh\left[\frac{\lambda x}{L}\right] \qquad \lambda=\sqrt{\frac{TL^2}{EI}} \qquad \{2\}$$

The majority of the literature focuses on searching for the appropriate four boundary conditions for the cambered web that could be used to solve for the coefficients *A*-*D* and define the steady-state lateral deformation w throughout the web span. Success has been achieved in defining the coefficients *A*-*D* for a web of uniform length across the width. The success was specific for web spans with a downstream misaligned roller and with an

aligned downstream roller with tapered radius in the CMD [2, 13]. There has been no success in developing boundary conditions that can be used to predict coefficients *A*-*D* for the case where a cambered web transits a web span between two aligned rollers. To date there is no closed form expression of the form {2} that predicts the lateral deformation of the cambered web toward the long side nor the magnitude of that deformation.

Swanson developed two methods to manufacture a cambered web. In his early tests [3], extra layers of films were strategically inserting near the core of a winding roll while winding uniform length webs. These rolls were then placed in an oven with high temperature for several hours to allow the web to deform due to viscoelastic material behavior. It is difficult to produce constant web camber using this method. Later Swanson developed a second method for producing camber by slitting the cambered web from a web of wider uniform length web [4]. Cambered sections of the web were cut followed by straight sections using two slitting blades mounted on a linear actuator that moved in the CMD. As a function of the web MD velocity and the CMD motion of the linear actuator a range of web camber radius could be produced. The lengths of the straight and cambered sections were slit 4 times longer than the test span length to ensure steady state conditions could be achieved. A web guiding system in a span immediately upstream of the test span controlled the lateral position of the elastic axis of the web as it entered the test span. Multiple edge sensors were placed throughout the test span such that the shape of the deformed cambered web could be measured. The straight sections of web allowed the nulls for the edge sensors to be determined prior to a cambered web section entering the test span. Dynamic lateral data was measured for the straight and cambered sections. The test results demonstrated that the downstream roller had to have a high friction coefficient with the polyester web to achieve measurable lateral steering toward the long side of the cambered web. This steering diminished with increased web tension. The high friction in the range of 2 to 4 was achieved by applying roller coverings (3M[1] 5461 or Tesa[2] 4863). In cases where the test rollers were bare aluminum, the friction coefficient was on the order of 0.3 and the lateral deformations were small, the cambered web deformed to an essentially straight web in the test section. It could be argued that the cambered web was being steered to straight geometry for these low friction cases. The investigators inferred that the cambered web was slipping throughout the web wrap of contact with the test span rollers and that the rollers had no consequence on the lateral deformation of the web. This inference resulted from witnessing increased friction coefficient did produce steerage.

Dynamic simulation has shown the first success in modelling the steerage of the cambered web. Fu [12] modeled the web with a series of straight and cambered sections per the tests described by Swanson [4] using Abaqus/Explicit[3]. Fu simulated a web position guide just upstream of the test span, similar to Swanson's test setup. As the cambered or straight web contacted the upstream roller, the guide maintained the lateral position of the elastic axis of the web at zero as it entered the test span. Fu's simulations were successful in producing steerage toward the long edge, but the fidelity of the simulation results was inadequate to capture the effect of web tension on steering witnessed in the tests. Improved simulations were conducted by Ren et. al. [13] using the standard dynamic implicit solution method in Abaqus. In these simulations a long section

[1] 3M Company, 2501 Hudson Rd, Maplewood, MN 55144, USA
[2] Tesa Tape Inc., 5825 Carnegie Boulevard, Charlotte, N.C. 28209, USA
[3] Dassault Systems, ABAQUS Simulia, Rising Sun Mills, 166 Valley St., Providence, RI 02909-2499

of straight web was modelled which wrapped the entry roller, proceeded through the test span, and then left the test span by wrapping and exiting an exit roller. In the beginning of the simulation constant MD web stress and velocity were achieved with no lateral steerage of the web. Then camber was induced only in the web in the test section by introducing a linear temperature variation across the web width. This resulted in a MD thermal expansion that varied linearly in the CMD and produced the camber slit into the web. The temperature variation was induced in the web using a UTEMP subroutine which began to affect web temperature half way through the wrap of the web about the upstream roller, continued through the test section and then was removed half way through the wrap of the web about the downstream roller. The thermally induced camber in the test section eliminated the need to simulate the web guide and provided the accuracy in results desired. The closed form expression {2} describing the lateral deformation of the cambered web was proven to be unobtainable. It was shown that the deformed radius of curvature of the web entering the downstream roller was required to solve for the coefficients of the equation. That deformed radius of curvature could be determined only by laboratory tests and dynamic simulation, thus a closed form expression was not possible.

Shelton's tests of cambered web steering [1] were conducted on cambered belts. The belts were cut by hand, spliced and tested on an existing web line [2]. A web guide maintained the lateral position of the web prior to entry to a test span where the steering was measured. Later tests were conducted on continuous webs where the camber was produced, the web guided to a null position followed by measurement of steering in a test span [3,4]. Web guides are installed at critical locations in roll-to-roll process machines whenever CMD web registration becomes critical. A critical location could be at a coating site or at a wound roll where edge alignment is necessary to prevent damage. Where does a cambered web steer while transiting several web spans between guides in a process machine? Does normal entry exist at any roller? Does the web continually steer towards the long edge until a web guide returns the lateral position of the web to an acceptable location?

This publication reports laboratory test and dynamic simulation results for a cambered web transiting two free spans separated by two idler rollers. The web is not guided. The intent is to study a case where there is no attempt to enforce any boundary conditions on the lateral displacement and slope of the web but to investigate the steering and boundary conditions that result.

EXPERIMENTAL SETUP AND RESULTS

The perfect web splice does not exist. There will always be a finite change in slope of the elastic axis of the web at the splice. Also there will be step changes in bending stiffness due to splice tape or web overlap and adhesive. A continuous cambered belt with no splice was cut from a wide polyester web supplied by Dupont[4] as shown in Figure 2. The web was first flattened and restrained on a vacuum bed. Two slitter blades were fixed at unique radial locations on an arm that was rotated manually to cut the belt. The web thickness was 0.0508 mm (0.002 in). Samples of web for material tests were cut on several axes. The web was found to be isotropic with measured modulus of 3.47 GPa (503 ksi) and Poisson's ratio of 0.3. The thermal expansion coefficient is 3.59×10^{-4} cm/cm/°C (2.16×10^{-5} in/in/F). The radius of curvature of the cambered belt as cut was 51.84 cm (20.41 in) and the width of the belt is 8.128 mm (0.32 in).

[4] Dupont Teijin Films, 3600 Discovery Drive, Chester, VA 23836, USA

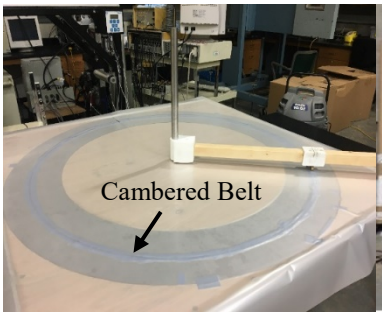

Figure 2 – Cambered belt

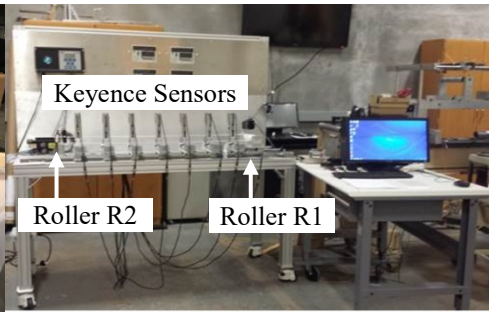

Figure 3 – Test apparatus

Several Keyence[5] LS-7010R edge sensors located in the test span to track for lateral movement of the cambered belt on the test bed (Figure 3). These sensors have measurement accuracy of 0.508 µm (0.00002 in) and 2400 data samples were recorded per second. All sensors were nulled prior to tests using a precision ground bar that rested and aligned with the two support rollers. The cambered belt was mounted on two cylindrical idler rollers. Roller R2 was a fixed idler. Roller R1 was aligned with roller R2 but was mounted on linear bearing ways. A cable was attached to the support of roller R1 and tension was induced in the web using by hanging dead weights on this cable. Roller R1 was driven in velocity control. The two rollers were nominally 154.94 cm (61 in) apart setting the web span length. The rollers were aligned within 25.4 µm (0.001 in) over their 20.3 cm (8.0 in) width but perfect alignment was not achievable. Even a small misalignment of these rollers will affect the lateral movement of a straight or a cambered belt.

The locations of the edge sensors in the test span are shown in Figure 4. The lateral displacements of the cambered belt measured by sensor S1 when the web tension was 10.41 N (2.34 lb) are shown in Figure 5. The web speed was set at 25.4 cm/s (10 in/s) and the friction coefficient between the web and the rollers were measured as 0.29. Sensor S1 measures the lateral displacement of the cambered belt near the end of the span prior to entry to roller R2. There are two choices when mounting the cambered belt on rollers R1 and R2. The cambered belt can be mounted with either the long edge to front (LTF) or with the long side to rear (LTR). The cambered belt would always move towards the longer edge provided the steering due to camber is greater than that due to roller misalignment, which was the case in these tests. To allow comparison of the slopes note that the absolute value of the measured deformations have been reported. The difference of the slopes of the data for the LTF and LTR cases in Figure 5 are indicative that rollers R1 and R2 were not perfectly aligned. Had the belt been perfectly slit and perfectly isotropic the edge deformation data in Figure 5 should have been nearly linear with respect to time. Since the perfect belt is likely nonexistent the decision was made to conduct LTF and LTR tests and average the results to null the effects of roller misalignment on the results.

[5] FS-V11, Keyence Corporation, 500 Park Boulevard, Suite 200, Itasca, IL 60143, USA.

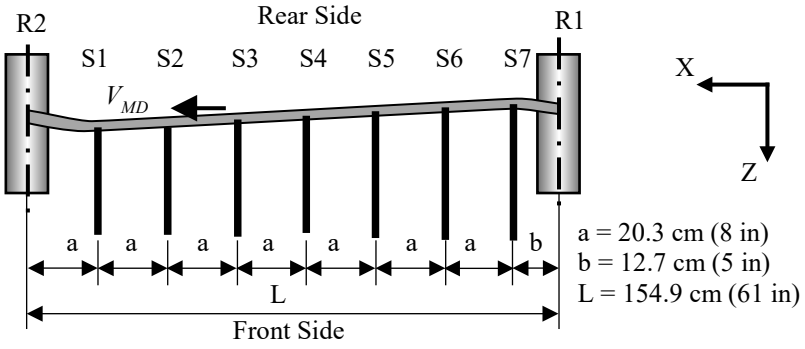

Figure 4 – Locations of edge sensors in the web span

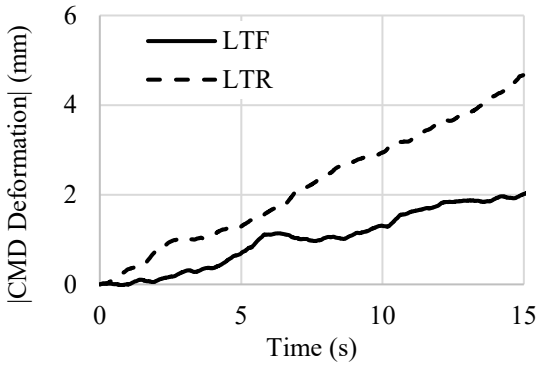

Figure 5 – Absolute CMD deformation from sensor S1, Tension=10.41 N (2.34 lb)

Initially the 7 edge sensors were intended to provide the deformed shape of the cambered web as it travelled from roller R1 to R2. It was found the method of setting the nulls of the sensors was inadequate and that when combined with the imperfections in the belt edges induced considerable error in the deformed shape. The decision was made to use all the sensors to infer the average lateral velocity of the belt.

Previous studies [4] had shown that increasing web tension produced less steering, presumably the result of elastically deforming the belt to a geometry closer to a straight belt. To explore the effect of tension, three test case tensions were chosen: 9.74, 10.41, and 11.97 N (2.19, 2.34 and 2.69 lb). The lowest tension was chosen as being sufficient to prevent any edge slackness. The highest tension was selected to prevent inelastic deformation. There were no trough or wrinkle instabilities in the range of tension chosen. Linear trend lines were regressed to the data for each sensor in Figure 6. The slope of the linear trend line provides the average lateral speed of the belt for a given sensor. The LTF lateral displacement data measured by the seven sensors when web tension is 10.41 N (2.34 lb) is shown in Figure 6(a). After conducting each experiment twice (Run 1 and Run 2) the average trend slopes from all sensors indicated the average LTF lateral speed was 0.1658 mm/s (0.0065 in/s). This is smaller than the LTR average lateral speed of 0.3020 mm/s (0.0119 in/s) from Figure 6(b). Since the LTR speed is almost twice as LTF speed, the effect of roller misalignment and other imperfections cannot be ignored. In

order to eliminate these effects, the lateral speed for the cambered web is defined as the average LTF and LTR speeds: (0.1658+0.3020)/2=0.2339 mm/s (0.0092 in/s). The MD velocity of the belt was 25.4 cm/s (10 in/s) and with a belt length of 325.7 cm (128.2 in), the period for the cambered belt to transit the machine is 12.8 s. There is evidence of this period in the data in Figure 6(a). The LTF lateral displacement data presented in Figure 6(a) was measured for 35 seconds which is about 2.7 belt cycles. The LTR data was collected for 15 seconds in Figure 6(b) for 1.2 belt cycles.

The slopes from the trend lines established from each sensor from Runs 1 and 2 are presented in the Appendix in Tables A1 through A3 for the three test tensions. Table A4 presents the average values of CMD velocity that were established by the method discussed in the previous paragraph. The data in Table A4 will be used for comparison to simulations.

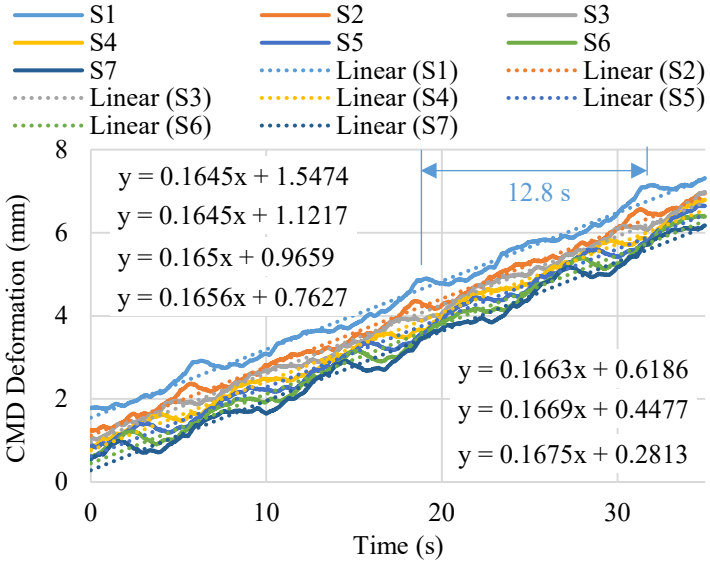

(a) LTF

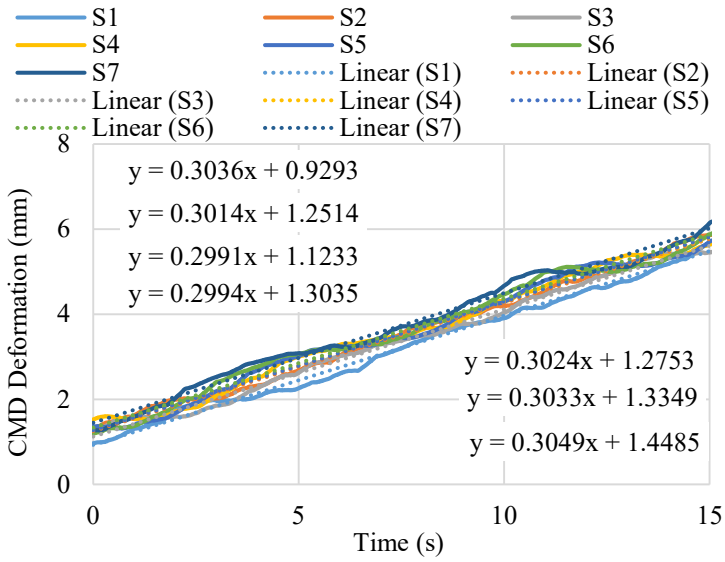

(b) LTR

Figure 6 – CMD deformations measured by 7 sensors, Tension=10.41 N (2.34 lb)

FINITE ELEMENT SIMULATION AND RESULTS

The web will be characterized in the simulations a constant thermal MD expansion coefficient and zero CMD expansion coefficient. The test apparatus used dead weights to induce web tension using roller R1 on linear ways. In the simulations, rollers R1 and R2 are modelled as rigid analytical surfaces that were allowed to rotate around their CMD cylindrical axes, otherwise these rollers were fully constrained. In the simulations web tension will be induced by decreasing the web temperature uniformly which will induce contact pressure between the web and rollers. The advantage to inducing web tension in the simulation by this method is that it simplifies the dynamics of the model and steady state tension is achieved and maintained rapidly. A linear temperature variation across web width was used to induce web camber. The web velocity is achieved by enforcing a constant angular velocity at roller R1. The simulation model uses shell elements (S4R) in Abaqus to model the web. Converged results were obtained when the S4R shell element dimensions were decreased to 0.8128 ×0.8128 mm^2 (0.032”×0.032”). The simulation assumed the web to be isotropic, the modulus was 3.47 GPa (503 ksi) and Poisson’s ratio of 0.3. A constant thermal expansion coefficient in the MD was set at 3.59×10^{-4} cm/cm/°C (2.16×10^{-5} in/in/F). The thickness of the cambered belt is 0.0508 mm (0.002 in) and the width is 8.128 mm (0.32 in). The web to be simulated has an initial radius of camber of 51.84 cm (20.41 in). The span length between the centers of rotation of rollers R1 and R2 was 154.94 cm (61 in) as shown in Figure 7(a). Both rollers have the same radius of 2.51 cm (0.99 in) and the friction coefficient between the web and the rollers was measured and set at 0.29. Roller R1 rotates with a constant MD velocity 25.4 cm/s (10 in/s).

The method to set the temperature changes to achieve the web tension and camber follows. The web was modelled as a straight belt residing at the CMD centers of rollers R1 and R2, subject to zero tension and ambient temperature. The belt was uniformly

partitioned into ten zones in the CMD direction with a linear temperature variation prescribed as shown in Figure 7. The unstressed radius of curvature r_0 of camber is defined in equation {3} where W is the web width and α is the MD thermal expansion coefficient. T_{high} is the highest change in temperature applied at one edge of the cambered belt in Figure 7(b) and T_{low} is the lowest change in temperature applied on the opposite edge:

$$r_0 = \frac{W}{\alpha\left(T_{high} - T_{low}\right)} \qquad \{3\}$$

The web tension T is related to the average temperature change in the web using equation {4}, where E is the web modulus and h is the web thickness:

$$T = -\alpha EWh\frac{T_{high} + T_{low}}{2} \qquad \{4\}$$

The highest and lowest temperature changes at the web edges can be determined by solving equations {3} and {4} simultaneously for desired values of the unstressed camber radius of curvature and the web tension required in the simulation. The cambered belt will not exhibit the desired unstressed radius curvature due in the simulations of tests due to web tension. To test the method a straight web with no restraints to restrict camber was simulated with the temperature variation calculated by equations {3} and {4} and the deformed shape of the web was explored. Per equation {3}, the stress free radius of curvature of the web is not a function of the web tension T, only temperature variation changes are important. The deformed radius of curvature was found to be 51.849 cm (20.413 in), only 0.015% different compared with the desired value of 51.841 cm (20.41 in). The thus method for inducing web camber with temperature change was verified.

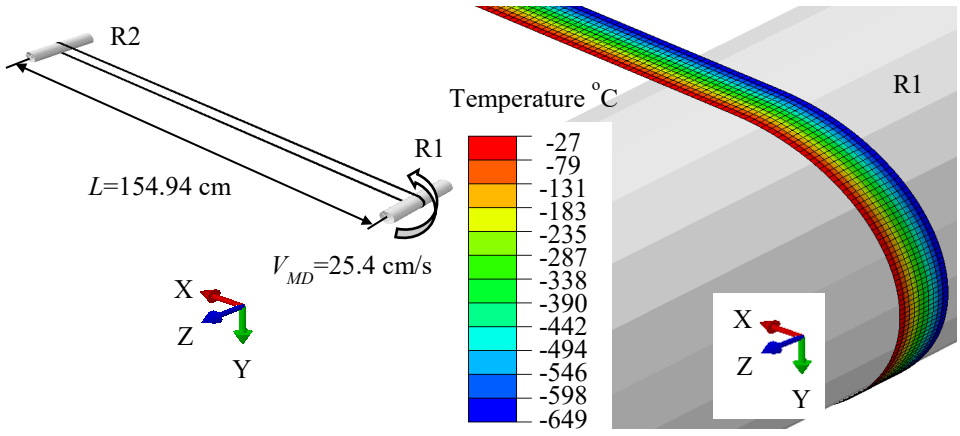

(a) Whole model (b) Temperature variation on R1

Figure 7 – Cambered belt FE model

In the cambered belt simulations the first step is to induce the temperature changes across the web width, roller R1 is not turning during this period of time. The tensioned cambered belt has varied MD membrane stress across web width due to the temperature

changes across the web width: the short edge has a greater MD stress while the long edge has a smaller MD stress as shown in Figure 8. The MD stress variation induces a counter-moment about the out-of-plane axis of the web, which reduces the initial curvature and the web appears straight in Figure 8. The MD tension of the cambered belt was calculated in simulation by averaging the nodal values of MD stress output across the web width and multiplying by the cross-sectional area (*Wh*). The result was 10.41 N (2.34 lb), which compares favorably with the desired test value of 10.41 N (2.34 lb).

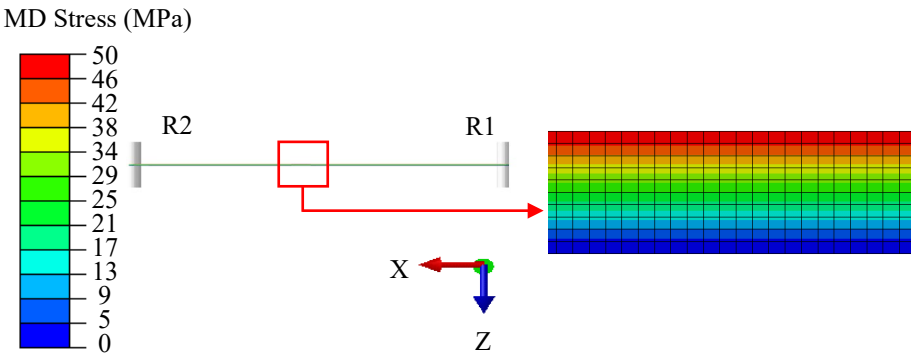

(a) Whole model (b) Web in section of free span

Figure 8 – MD stress of the cambered belt after pretension

The temperature changes that resulted in the stresses shown in Figure 8 were applied to the web during the first second in the simulation. During the next second, the angular velocity of roller R1 was increased from zero to 10.101 rad/s and then remained constant through the duration of the simulation. Due to the contact pressure between the web shell elements and the rigid rollers, which resulted from the web tension which was created by the temperature change, and friction between the web and roller R1 the web will move in the MD. In steady state the web achieves the velocity of 25.4 cm/s (10 in/s) which corresponds to the value in tests specified earlier.

The cambered web steers toward the long edge in all simulations. The lateral displacement of the elastic axis of the web is shown in Figure 9. At t=0 s in Figure 9 the pretension step has been completed and the web begins to move. The deformed shape of the cambered web was determined by the initial curvature, the web properties, the MD tension and the interactions between web and rollers. The web acquires a steady deformed shape in space in a very short time; note the deformed shapes are very similar after 1, 2 and 3 seconds of simulation. The belt may have a steady deformed shape but it is moving at constant speed in the CMD toward the long side of the belt.

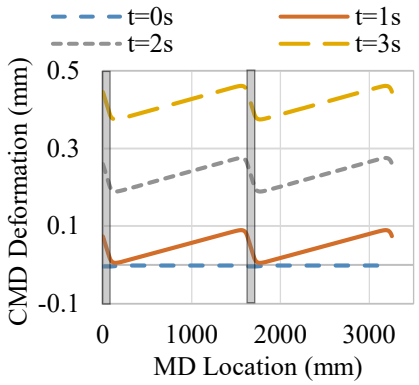

Figure 9 – Lateral displacement of the cambered belt when tension is 10.41 N (2.34 lb)

The lateral displacements (Figure 9), slopes (Figure 10) and curvatures (Figure 11) are indicative the cambered web reaches a steady state deformed condition in 2 seconds. The slope and curvature data presented in Figs. 10 and 11 were obtained using finite difference central difference approximations of derivatives of the lateral deformation data on the elastic axis of the web. The left grey bar in figures indicates the location of roller R1 and the second bar is for roller R2 in Figure 7(a). In the steady state condition, the web enters the rollers non-normally, as indicated by the nonzero slopes in Figure 10. The web has negative slopes on the rollers and the slope becomes positive in the free span due to the S deformed shape (Figure 9).

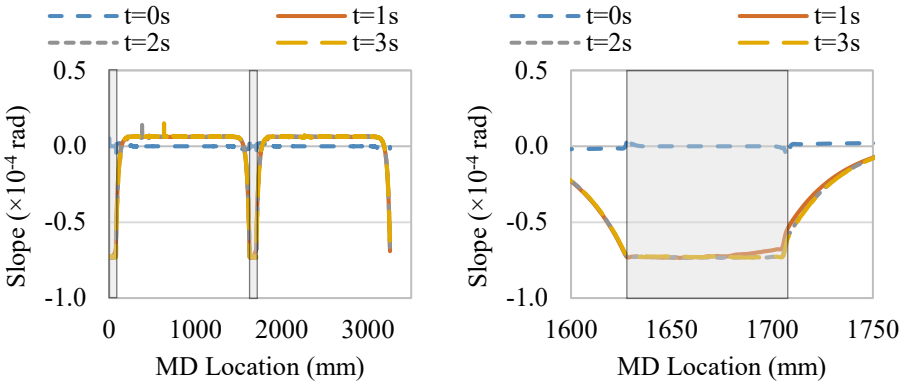

(a) Whole web (b) Web on roller R2

Figure 10 – Slope of the cambered belt when tension is 10.41 N (2.34 lb)

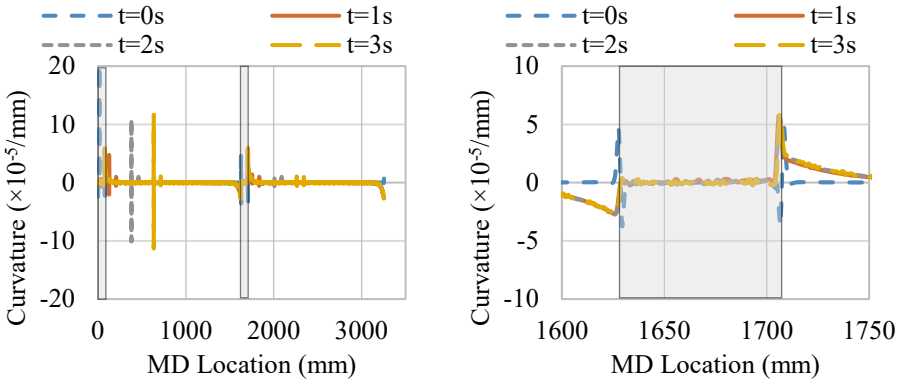

(a) Whole web (b) Web on roller R2

Figure 11 – Curvature of the cambered belt when tension is 10.41 N (2.34 lb)

The curvatures presented in Figure 11 require further explanation. In beam theory curvature is related to bending moment *M(x)*, bending stiffness *EI* and the radius of curvature ρ:

$$\frac{d^2w}{dx^2} = \frac{M(x)}{EI} = \frac{1}{\rho} \qquad \{5\}$$

The MD stresses after 3 seconds of simulation are shown in Figure 12 with obvious MD stress variation across the web width. Bending moment is defined in terms of internal stresses as:

$$M = \int_{-W/2}^{W/2} \sigma_{MD} z h dz \qquad \{6\}$$

The MD stresses in Figure 12 vary as a function of *z* location in the web on roller R1. From equation {6} it would appear the bending moment in the web is non-zero and that from equation {5} that the curvature should also be non-zero. In Figure 11(b) the curvature appears to be zero in the web on the roller but is not. In the stress-free state this web has a radius of curvature r_0 of 51.841 cm. In the deformed state the web has been straightened on roller R1 but an internal moment has been induced $M=EI/r_0$=0.0152 N-m. This induces a linear variation in MD stress per elementary beam theory:

$$\sigma_{MD} = -\frac{Mz}{I} + \frac{T}{A} = -\frac{12Mz}{hW^3} + \frac{T}{hW} \qquad \{7\}$$

For this test case, equation {7} would predict a linear stress variation from -1.98 to 52.4 MPa over the web width which compares nicely with the stresses in the legend of Figure 12. Thus in the deformed state the web has no curvature in Figure 11 as it transits roller R1, but originally in the unstressed state the web had a camber radius. To straighten the web on R1 as seen in Figures 9, 10 and 11 required a bending moment.

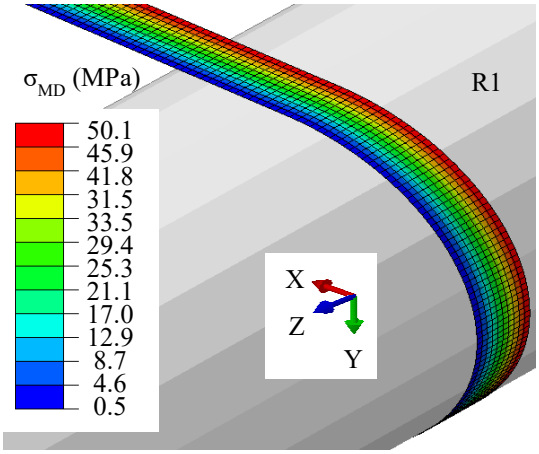

Figure 12 – MD web stresses in web on R1 and exiting into the free

The entry and exit slopes of the web never become zero in Figure 10, normal entry is not achieved. This non-normal entry is the fundamental reason the cambered belt steers on a cylindrical roller. If the cambered web travels onto a cylindrical roller with a MD velocity V_{MD} and a negative angle θ as shown in Figure 13, the web would steer to the positive z direction. The steering speed V_{steer} and amount of steerage U_{steer} can be determined as:

$$V_{steer} = V_{MD} * \tan(\theta) \quad \{8\}$$

$$U_{steer} = V_{MD} * \tan(\theta) * \Delta t \quad \{9\}$$

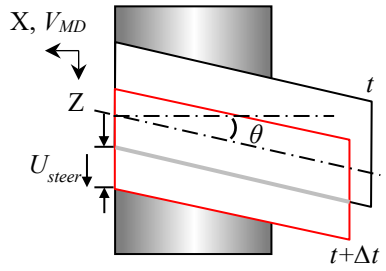

Figure 13 – Deformed cambered web at time t and time $t+\Delta t$

The average lateral speed of the cambered belt can be determined by two methods in the simulations. The first method would employ equation {8}. The simulations can be used to estimate the slope of the web on the roller and the web MD velocity is known. The slope is quite constant as the web on the rollers in Figure 10(b), about 0.00073 rad. The steering velocity V_{steer} from equation {8} is 0.0185 cm/s (0.00730 in/s). The second method is to query the CMD speed for a specific web node in the simulations. A node located on the elastic axis of the cambered web was chosen and the lateral velocity

converges to a steady value of 0.0195 cm/s (0.00768 in/s) in 2 seconds as shown in Figure 14, a 5.4% difference compared with the value from the first method.

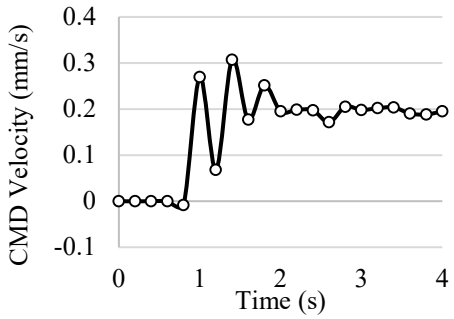

Figure 14 – CMD velocity of a node at web elastic axis

Abaqus also allows slippage to be explored. The contact status of the cambered belt shows the web has small area of slip at entry and a larger slip zone near the exit zone for both rollers R1 and R2 in Figure 15. The green contact status of the long edge with lower tension (Figure 12) indicate slipping across whole roller path. The cambered belt has a larger slipping zone at the exit compared with the entry location. Note at entry to the roller the slope of the web (Figure 10) at the end of the free span and the slope of the web on the roller are equal (about -0.00073 rad). At the exit a near step decrease in slope is witnessed from -0.00073 rad in the web on the roller to about -0.00057 rad for the web in the free span, this is allowed by the large zone of slip near the exit.

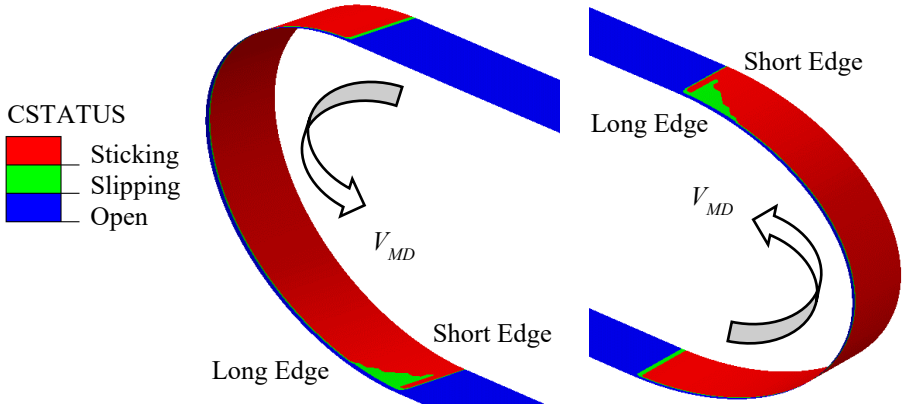

(a)Web on roller R2 (b) Web on roller R1

Figure 15 – Contact status when tension is 10.41 N (2.34 lb)

Increased web tension acts to diminish both the lateral deformations of the web in the free span and the entry slope of the web to the rollers as shown in Figure 16.

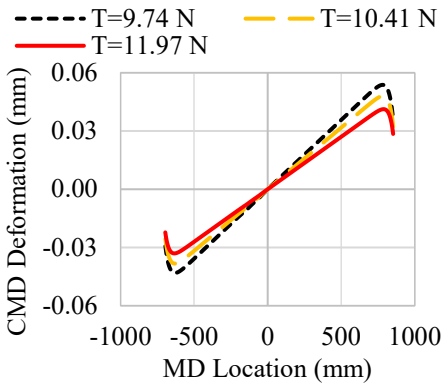

Figure 16 –Effect of tension on lateral displacement of web span between R1 and R2.

RESULTS

The results from tests and simulations are presented in Table 1. The agreement between the lateral velocities measured in tests in comparison to simulations is good. With this agreement the output from the dynamic simulation can be used to study other behaviors with confidence. Steerage is usually defined as the amount of lateral deformation that occurs in a free span between entry and exit. Although this can be witnessed graphically in Figure 16, this is presented in greater accuracy in Table 1. The steerage is obviously not large per the definition given. Perhaps for the case of the cambered belt the steerage is better defined by the steering velocity and the related entry slope to the downstream roller (R2). Every point on the elastic axis of a cambered belt is moving laterally in the CMD through time.

	CMD Lateral Steering Velocity			Steerage	R2 Entry Slope
Tension (N)	Test (mm/s)	Simulation (mm/s)	% Error	Simulation (mm)	Simulation (rad)
9.74	0.2540±0.0106	0.2261	12.3%	0.0644	0.00081
10.41	0.2257±0.0035	0.1956	15.4%	0.0575	0.00073
11.97	0.1527±0.0058	0.1727	-11.6%	0.0502	0.00064

Table 1 – CMD Speed of the Cambered Belt

At an instant in time the deformed shape of the free span (Figure 16) could be represented by equation {2} if the coefficients A, B, C and D could be determined. From the simulations w_i, θ_i, w_j and θ_j can be determined at an instant in time and A-D could be determined but simulation was required to determine the boundary conditions. Curvature boundary conditions could also be used. In Figure 11(b) it is obvious that $\frac{d^2 w_i}{dx^2}$ and $\frac{d^2 w_j}{dx^2}$ are unique and are affected by the slippage witnessed in Figure 15. Thus w_i might be arbitrarily assumed to be zero but other boundary conditions such as θ_i, w_j, θ_j, $\frac{d^2 w_i}{dx^2}$

and $\frac{d^2 w_j}{dx^2}$ would have to be inferred or determined by tests or simulations. It is concluded similar to Ren et. al. [13] that no closed form solutions in the form of equation {2} are possible, whether the cambered web is continuous or in the form of a belt.

CONCLUSIONS

The lateral dynamics of a cambered belt has been investigated by tests and dynamic simulations with good agreement. It is concluded that no closed form solutions exist for this problem. Qualitatively it can be concluded that the cambered belt does steer toward the long edge of the web in terms of a small steerage and a larger steering velocity. When combatting lateral registration problems with cambered webs guiding is required to ensure the web will be on target for processing.

REFERENCES

1. Shelton, J. J., "Effects of Web Camber on Handling," Proceedings of the 4th International Conference on Web Handling, Web Handling Research Center, Stillwater, Oklahoma, June, 1997, pp. 248-263.
2. Shelton, J. J., "Lateral Dynamics of a Moving Web," Ph.D. Dissertation, Oklahoma State University, July 1968.
3. Swanson, R. P., "Mechanics of Non-Uniform Webs," Proceedings of the 5th International Conference on Web Handling, Web Handling Research Center, Stillwater, Oklahoma, June, 1999, pp. 443-459.
4. Swanson, R. P., "Lateral Dynamics of Non-Uniform Webs," Proceedings of the 10th International Conference on Web Handling, Web Handling Research Center, Stillwater, Oklahoma, June, 2009, pp. 531-554.
5. Olsen, J. E., "Lateral Mechanics of an Imperfect Web," Proceedings of the 6th International Conference on Web Handling, Web Handling Research Center, Stillwater, Oklahoma, June, 2001, pp. 457-468.
6. Olsen, J. E., "Lateral Mechanics of an Imperfect Web," Journal of Pulp and Paper Science, Vol. 28, Sep, 2002, pp. 310-314.
7. Benson, R. C., "Lateral Dynamics of a Moving Web with Geometrical Imperfection," Journal of Dynamic Systems, Measurement, and Control, Vol. 124, March, 2002, pp. 25-34.
8. Olsen, J. E., "Shear Effects and Lateral Dynamics of Imperfect Webs," Proceedings of the 7th International Conference on Web Handling, Web Handling Research Center, Stillwater, Oklahoma, June, 2003, pp. 119-131.
9. Olsen, J. E., "Lateral Mechanics of Baggy Webs at Low Tensions," Proceedings of the 8th International Conference on Web Handling, Web Handling Research Center, Stillwater, Oklahoma, June, 2005, pp. 25-37.
10. Brown, J. L., "Effects of Concave Rollers, Curved-Axis Rollers and Web Camber on the Deformation and Translation of a Moving Web," Proceedings of the 8th International Conference on Web Handling, Web Handling Research Center, Stillwater, Oklahoma, June, 2005, pp. 61-80.
11. Jones, D. P., "Web Sag and the Effects of Camber on Steering," Proceedings of the 9th International Conference on Web Handling, Web Handling Research Center, Stillwater, Oklahoma, June, 2007, pp. 353-370.

12. Fu, B., and Good, J. K., “Explicit Simulations of Cambered Web Steering,” Proceedings of the 13th International Conference on Web Handling, Web Handling Research Center, Stillwater, Oklahoma, June, 2015.
13. Ren, Y., Shi, J., and Good, J. K., “Lateral Deformation of Webs Transiting Spans in Roll-to-roll Process Machines,” ASME Journal of Dynamic Systems Measurement and Control, accepted.

APPENDIX

	T=9.74 N			
	LTF (mm/s)		LTR (mm/s)	
	Run1	Run2	Run1	Run2
S1	0.1326	0.1549	0.3655	0.3350
S2	0.1336	0.1562	0.3716	0.3546
S3	0.1344	0.1570	0.3556	0.3823
S4	0.1349	0.1580	0.3348	0.4110
S5	0.1351	0.1585	0.3134	0.4227
S6	0.1364	0.1610	0.3061	0.4064
S7	0.1379	0.1613	0.3139	0.3874

Table A1 – Lateral Test Velocities, T=9.74 N

	T=10.41 N			
	LTF (mm/s)		LTR (mm/s)	
	Run1	Run2	Run1	Run2
S1	0.1645	0.1415	0.3036	0.2939
S2	0.1645	0.1422	0.3014	0.2946
S3	0.1650	0.1430	0.2991	0.2934
S4	0.1656	0.1440	0.2994	0.2913
S5	0.1663	0.1440	0.3024	0.2891
S6	0.1669	0.1453	0.3033	0.2888
S7	0.1675	0.1468	0.3049	0.2885

Table A2 – Lateral Test Velocities, T=10.41 N

	T=11.97 N			
	LTF (mm/s)		LTR (mm/s)	
	Run1	Run2	Run1	Run2
S1	0.0940	0.0643	0.2283	0.2090
S2	0.0950	0.0658	0.2294	0.2134
S3	0.0983	0.0665	0.2334	0.2139
S4	0.1019	0.0663	0.2375	0.2121
S5	0.1041	0.0658	0.2388	0.2103
S6	0.1031	0.0655	0.2367	0.2090
S7	0.1001	0.0664	0.2350	0.2108

Table A3– Lateral Test Velocities, T=11.97 N

	T=9.74 N	T=10.41 N	T=11.97 N
Average CMD velocity (mm/s)	0.2540	0.2257	0.1527
Standard deviation (mm/s)	0.0106	0.0035	0.0058

Table A4 – Average Lateral Test Velocities